参赛学生姓名： 周子涵、许知微、颜子皓

中学： 重庆市巴蜀中学校

省份： 重庆市

国家/地区： 中 国

指导老师姓名： 范 兴 、王 旭

指导老师单位： （范兴）重庆大学化学化工学院

（王旭）重庆市巴蜀中学校

论文题目： Scalable Fabrication of Nano-Arrayed ZnO/Cotton Composite Fibers for Human-Robot Interactive Fabric

2026 S.T.Yau High School Science Award
仅用于2026丘成桐中学科学奖论文公示

Scalable Fabrication of Nano-Arrayed ZnO/Cotton Composite Fibers for Human-Robot Interactive Fabric

Zihan Zhou, Zhiwei Xu, Zihao Yan

Abstract

Electronic fibers have emerged as a promising wearable sensing technology for human-centered interaction owing to their softness, breathability, and conformal adhesion. Although nano-arrayed structures have demonstrated their effectiveness in improving sensor performance, their formation generally relies on direction-selective crystal facet growth under extreme pressure or temperature conditions, which limits the scale-up of material production. Herein, we present an electric field-induced selective crystal facet growth strategy that enables the scalable fabrication of nano-arrayed oxide/polymer composite fibers at room temperature and atmospheric pressure. According to which, a cotton wire coated with a ZnO nanoneedle array was fabricated on a meter scale by simply introducing an auxiliary electrode into a continuous-flow fiber coating process. It was then woven as a fully addressable haptic fabric for wearable kinesthetic communication and human–metaverse interfaces. The sensitivity increased by 50% owing to the nano-array structure and remained almost unchanged over 2000 bending cycles. Mirrored interaction between a small robot and human motion was demonstrated by wearing such a fabric. This strategy can also be applied to other fiber materials, paving the way for commercial applications of electronic fabrics in fields like embodied intelligence.

Keywords

Electronic fabric; Flexible sensor; Nano-arrayed ZnO; Composite fiber; Scalable fabrication; Human-machine interaction

2026 S-T Yau High School Science Award
仅用于2026丘成桐中学科学奖论文公示

Contents

1. Introduction 4

2. Results and Discussion 5

2.1 Structure design of the composite fiber and the sensing fabric 5

2.2 Effect of the electric field on the nano-arrayed ZnO structure 8

2.3 Continuous fabrication of the fiber-type sensor 9

2.4 Demonstration of the sensing fabric 12

3. Conclusions 15

4. Experimental section 16

4.1 Continuous fabrication of ZnO composite fibers 16

4.2 Fabrication of wire-type tensile stress sensors 16

4.3 Weaving process for the sensing fabric 16

4.4 Characterizations and measurements 17

5. References 18

6. Acknowledgements 21

2026 S.-T. Yau High School Science Award
仅用于2026丘成桐中学科学奖论文公示

1. Introduction

The continuous advances in flexible electronics are profoundly reshaping the landscape of human–machine interaction, VR/AR, and personalized healthcare[1,2]. Among these, flexible wearable sensors, distinguished by their exceptional deformation compliance and biocompatibility, have become an important hardware foundation for human physiological signal acquisition, with a global market exceeding US$6.23 billion[3–5]. With the recent rapid development of smart healthcare, embodied intelligence, and other related fields, flexible sensors are facing new challenges, such as long-term wearability, in-situ monitoring, and multi-site high-precision monitoring[6–9]. Therefore, emerging electronic fabrics with addressable haptic sensing functions have attracted considerable attention. Such fabrics are usually woven from micro/nano functional-structured composite fibers, which are fabricated by depositing piezoelectric, piezoresistive, or dielectric semiconductors onto substrates such as fibers, yarns, or others[10–14]. These materials can simultaneously offer softness, breathability, stretchability, and conformal adhesion, making them suitable for non-invasive physiological signal acquisition[15–20].

To improve the sensitivity and addressable precision of composite fibers, array structures such as nanoneedles and nanorods were introduced into the oxide or polymer semiconductor layer on the composite fiber surface, thereby significantly improving both sensitivity and addressable precision[21–23]. However, most nano-array structures are fabricated under high-pressure or high-temperature conditions, such as hydrothermal conditions, to selectively enhance growth reaction along different crystal-facet directions. Such extreme reaction conditions are incompatible with scalable fabrication, especially for roll-to-roll processing on long fiber substrates[24,25].

Herein, we proposed an electric field-induced selective crystal facet growth strategy

2026 S.T. Yau High School Science Award
仅用于2026丘成桐中学科学奖论文公示

that enables the scalable fabrication of nano-arrayed oxide/polymer composite fibers at room temperature and atmospheric pressure. Using this strategy, a cotton wire coated with a ZnO nanoneedle array was fabricated at the meter scale by simply introducing an auxiliary electrode into a continuous-flow fiber coating process. It was then woven into a fully addressable haptic fabric for wearable kinesthetic communication and human-metaverse interfaces. The sensitivity increased by 50% owing to the nano-array structure and remained almost unchanged over 2000 bending cycles. By wearing such a fabric, mirrored interaction between a small robot and human motion was demonstrated. This strategy can also be applied to other fiber materials, paving the way for commercial applications of electronic fabrics in fields such as embodied intelligence.

2. Results and Discussion

2.1 Structure design of the composite fiber and the sensing fabric

Figure 1 systematically illustrates the structure design of the composite fiber and the sensing fabric. As shown in **Figure 1a, 1b**, to perform a human–machine interaction action, we need to collect tactile and motion states from different parts of the human body. Therefore, long-length fibers are required for large-area fabric processing. Each fiber interweaving node in the fabric can serve as a pixel. At each interweaving node, nanostructures can affect the contact resistance of the micro-interface, thereby affecting sensing sensitivity. However, as sensing expands from localized areas such as the hand to the entire human body, the number of sensing points will also increase quadratically or even geometrically, which makes it difficult for us to precisely scalable fabricate and align the sensing nodes. (**Figure 1c**).

The scalable fabrication of nano-structured sensing nodes is essentially the selective growth of nanostructures. Traditional fabrication requires high temperature and high

2026 S. T. Yau High School Science Award
仅用于2026丘成桐中学科学奖论文公示

pressure to activate intermediate concentrations to achieve direction-selective crystal facet growth. However, such regulation possesses low reaction efficiency. To realize a green and efficient fabrication approach, we proposed an external electric field-induced selective crystal facet growth strategy. For which, the electric field can alter intermediate concentrations through electromigration, avoiding extreme reaction conditions. More importantly, the electric field can induce the selective growth of crystal facets.

As shown in **Figure 1d**, we coated semiconducting ZnO nanoneedle arrays with CNT/PVDF material that has a flexible polymer conductive network structure. For which, the ZnO nanoneedle array ensures conductive discontinuity in the axial direction. This guarantees addressing accuracy. In the radial direction, the oxide helps charges retain a certain separation capability. On the other hand, in the upper polymer conductive network composite, hydrogen bonding between hydroxyl groups and fluoride ions ensures the connection between CNT and PVDF. The contact between flexible polymer chains and the nanoneedle array also ensures that even under a very small force, large contact deformation can be generated on the nanoneedles to improves sensitivity.

The growth mechanism of the ZnO nanoneedle arrays is illustrated in **Figure 1e**. We designed a continuous-flow reaction bath for electrically assisted deposition to facilitate the scalable fabrication of ZnO nanocomposite fibers. Under an applied electric field, positively charged $Zn(OH)_2$ colloidal particles migrate electrophoretically toward the cathode, gradually interconnecting and undergoing gelation to form a network. Once the $Zn(OH)_2$ concentration at the surface of the fiber cathode exceeds a critical value, ZnO nucleates and continues to grow, ultimately forming ZnO nanoneedle arrays on the fiber surface. **Figure 1f** reveals the regulation of ZnO growth orientation by the

2026 S.-T. Yau High School Science Award
仅用于2026丘成桐中学科学奖论文公示

external electric field from a crystallographic perspective. In the absence of an electric field, $Zn^{2+}$and O^{2-} are alternately arranged along conventional pathways, and the lattice exhibits disordered or isotropic growth. Upon application of an electric field, the field direction is aligned with the [0001] crystallographic direction, and $[Zn(OH)_4]^{2-}$ complex ions appear in the system. The electric-field force drives selective adsorption and rearrangement on specific crystal facets, inducing preferential growth of ZnO along the [0001] direction. This selective growth of crystal facets induced by the external electric field effectively produces vertically aligned ZnO nanorod/nanoneedle arrays.

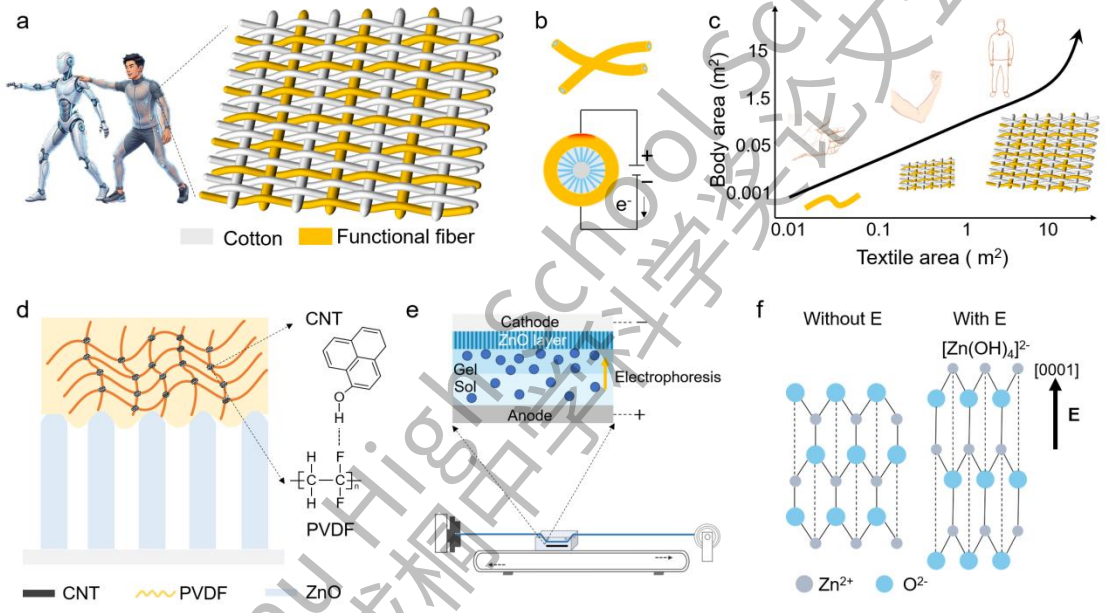


Figure 1. Structure design of the composite fiber and the sensing fabric. (a) Schematic illustration of the sensing fabric structure and its application in human–machine interaction. (b) Schematic illustration of the sensing mechanism. (c) Area scalability of the sensing fabric from micro-devices to macroscopic human body coverage. (d) Schematic illustration of the interface structure and chemical interactions between the ZnO nanoarray and the CNT/PVDF sensing layer. (e) Schematic diagram of the electric-field-assisted continuous deposition apparatus and the electrophoretic deposition process on the fiber surface. (f) Comparative schematic of ZnO nucleation behavior and crystal facet orientation with and without the external electric field.

2026 年 T.Yau High School Science Award 仅用于2026年成相中学科学论文公示

2.2 Effect of the electric field on the nano-arrayed ZnO structure

Figure 2 presents a systematic investigation of the effect of the electric field on the nano-arrayed ZnO structure. As shown in **Figure 2a**, we found that the electric field affects the nanomorphology of ZnO. Specifically, at a relatively low voltage of 1 V, the ZnO nanostructures exhibited a sparsely distributed short-rod morphology. When the voltage increased to 3 V, they exhibited a densely distributed, slender nanoneedle morphology. When the voltage increased to 5 V, they exhibited a thick nanorod morphology (**Figure 2b**).

To investigate the factors influencing the morphology of the ZnO nanostructures, we further examined the effects of precursor concentration on the diameter and length of the nanoarrays. As shown in **Figure 2c**, the average diameter of the ZnO grains increased continuously with increasing zinc ion precursor concentration. The grain length initially increased rapidly, reaching a maximum at a concentration of approximately 0.02 mol/L, and then decreased markedly as the zinc ion concentration increased further. These results indicate that the geometry and spatial arrangement of the ZnO nanoarrays can be effectively controlled by adjusting parameters such as the precursor concentration.

Based on these morphological differences, we compared the sensitivities of sensors without ZnO nanostructure modification and sensors modified with four types of ZnO nanostructures: short rod, needle, long rod, and sheet. As shown in **Figure 2d**, the densely distributed, slender nanoneedle morphology exhibited the highest relative resistance change. These results indicate that nano array structure with high aspect ratios and uniform alignment can increase sensitivity by 50%, owing to maximize changes in contact area and piezo potential effects under mechanical loading. Finally,

2026 S.-T. Yau High School Science Award
仅用于2026丘成桐中学科学奖论文公示

Figure 2e examines the monotonically increasing relative resistance change of the sensor over a wide strain range of 0 – 80%. The results indicate that the optimized composite fiber structure combines high sensitivity with a wide detection range.

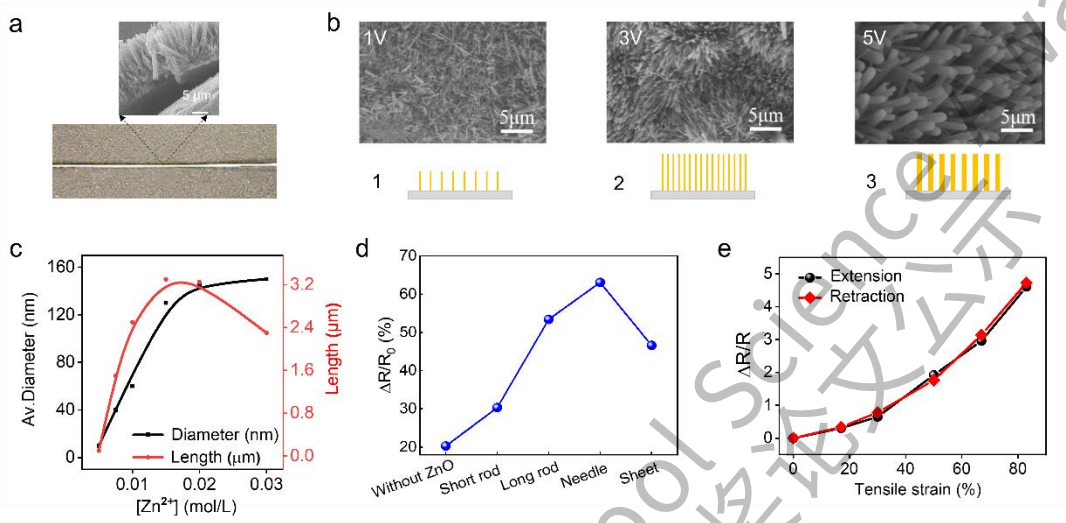


Figure 2. Effect of the electric field on the nano-arrayed ZnO structure. (a) Macroscopic photograph and surface SEM morphology of the ZnO-based composite fiber. (b) SEM images and corresponding structural evolution schematics of ZnO nanostructures grown at different voltages (1 V, 3 V, and 5 V). (c) Effects of Zn^{2+} concentration on the average diameter and length of ZnO nanostructures. (d) Effect of different ZnO morphologies on the sensitivity ($\Delta R/R_0$) of the fiber sensor. (e) Resistance response of the sensor under tensile strain from 0% to 83% and its stability during extension–retraction cycles.

2.3 Continuous fabrication of the fiber-type sensor

Figure 3 systematically validates the feasibility of the continuous fabrication of the fiber-type sensor based on the nano-arrayed ZnO composite fibers. As shown in **Figure 3a**, the nano-arrayed ZnO composite fiber is continuously coated with a CNT/PVDF composite polymer layer by an automatic coating device, thereby achieving continuous fabrication of fiber-type sensor units on meter-scale long fibers. **Figure 3b** schematically illustrates the interfacial interaction between CNT and PVDF. CNTs

2026 S. T. Yau High School Science Award
仅用于2026丘成桐中学科学奖论文公示

grafted with hydroxyl (-OH) functional groups on their surfaces are dispersed in the PVDF matrix. The hydrogen atoms in the functional groups on the CNT surface form hydrogen bonds with the fluorine atoms on the PVDF molecular chains. Specifically, the hydroxyl groups modified on the CNT sidewalls act as hydrogen bond donors, while the highly electronegative fluorine atoms in the PVDF units act as hydrogen bond acceptors. This hydrogen bonding enhances the interfacial adhesion between CNT and PVDF, improves the stress transfer efficiency at the filler-matrix interface, and regulates the electron transport properties of the composite. At the macroscopic level, the carbon nanotube network is embedded within the continuous PVDF matrix, and the interconnected nanotubes build a flexible conductive network.

Next, we systematically optimized the performance of the fiber-type sensor. First, we investigated the effect of polymer coating thickness on sensing sensitivity. As shown in **Figure 3c**, the sensing responses of fiber-type sensor with coating thicknesses ranging from 3 to 11 μm were evaluated using the relative resistance change, as the evaluation metric. The results showed a pronounced inverted U-shaped dependence of $\Delta R/R_0$ on coating thickness. As the thickness increased from 3 to 7 μm, $\Delta R/R_0$ increased continuously and reached its maximum at 7 μm. Further increases in thickness to 9 and 11 μm resulted in a gradual decrease in $\Delta R/R_0$. These results indicate that 7 μm is the optimal coating thickness for this composite system.

Then, we investigated the real-time current response of the fiber-type sensor under different tensile strains. As shown in **Figure 3d**, stepwise tensile strains of 0%, 17%, 30%, 50%, 67%, and 83% were applied sequentially, with each strain level maintained for approximately 10 s while the current was recorded throughout the process. The results showed that the current decreased stepwise with increasing strain. The current was approximately 2.35 mA at 0% strain, decreased sharply to approximately 1.15 mA

2026 S. T. Yau High School Science Award
仅用于2026丘成桐中学科学奖论文公示

at 17% strain, and further decreased to approximately 0.58 mA at 30% strain. Thereafter, the decrease became substantially less pronounced, with current values of approximately 0.45 mA at 50% strain, 0.35 mA at 67% strain, and 0.33 mA at 83% strain. The current remained stable at each strain plateau without apparent drift, indicating good responsiveness of the composite fiber to tensile strain.

Finally, we investigated the stability of the fiber-type sensor under repeated bending. **Figure 3e** presents the electrical output of the fiber-type sensor over 2,500 bending cycles. The results showed that the resistance initially increased rapidly and then more slowly as the number of bending cycles increased. The initial resistance at 0 cycles was approximately 18.3 kΩ. Beyond 2,000 cycles, the resistance largely reached a plateau, attaining approximately 22.0 kΩ. The cyclic bending stability test confirmed that the coating structure provides strong interfacial adhesion between the conductive layer and the substrate, and effectively mitigates stress concentrations during repeated deformation.

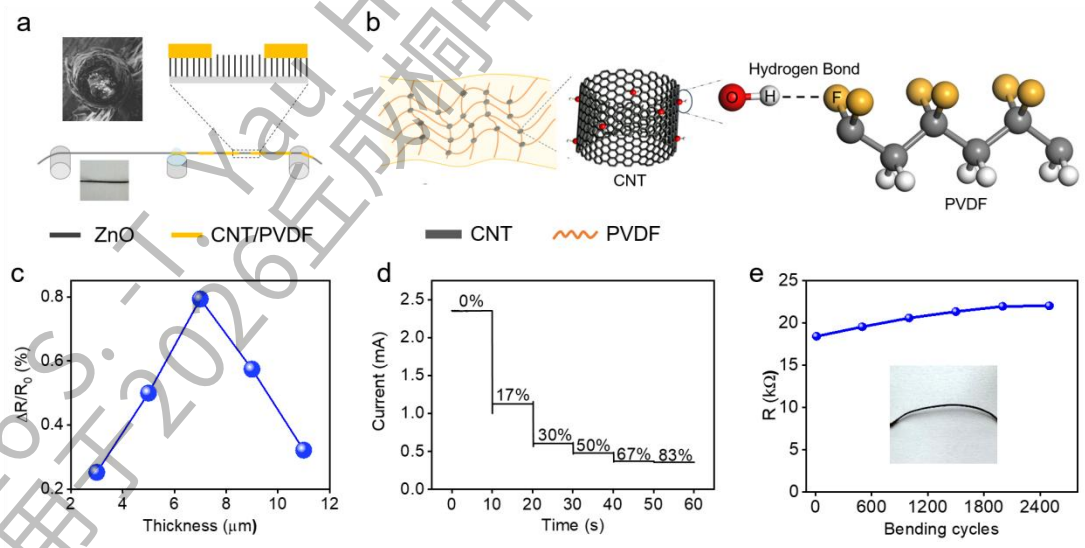


Figure 3. Continuous fbrication and prformance optimization of the fiber-type sensor. (a) Schematic illustration of continuous fbrication and cross-sectional SEM

2026年3月 Yau High School Science Award
仅用于2026丘成桐中学科学奖公示

image of the fiber. (b) Schematic diagram of the hydrogen bonding interactions within the CNT/PVDF network. (c) Relative resistance change ($\Delta R/R_0$) as a function of sensing layer thickness. (d) Current response of the sensor under stepped strains ranging from 0% to 83%. (e) Resistance variation of the sensor over 2400 bending cycles; the inset shows a photograph of the sensor in a bent state.

2.4 Demonstration of the sensing fabric

To demonstrate the fiber-type sensor in wearable sensing fabric, we fabricated a sensing fabric using a flying-shuttle weaving technique and evaluated its array sensing performance and potential future applications. As shown in **Figure 4a, b**, a 30 cm × 30 cm sensing fabric was fabricated by flying-shuttle weaving. Spacer yarns were introduced into the interlaced structure to secure each sensing unit between adjacent interwoven cotton yarns, preventing sliding and deformation of neighboring fibers. This configuration maintained a high degree of structural stability and enabled individual addressability and zero crosstalk between adjacent sensing units. Theoretically, when composite fibers with a diameter of 0.2 mm are used as the warp, cotton threads as the weft, and cotton threads are further used as spacer threads between two adjacent warp threads, a fabric woven by an interlaced shuttle-weaving method can achieve a resolution of 0.25 mm. A 3 × 3 array of sensing nodes was selected to evaluate the sensing signals and crosstalk suppression capability. When individual nodes at different locations on the sensing fabric were randomly selected and pressed one at a time, electrical signals were generated at the corresponding nodes. When any two adjacent sensing nodes were pressed simultaneously, electrical signals were generated at the corresponding nodes without crosstalk signals. When any three adjacent sensing nodes were pressed simultaneously, no non-crosstalk signals were observed, confirming the ability of the fabric sensing array to effectively distinguish external mechanical stresses and suppress crosstalk.

2026 S. T. Yau High School Science Award
仅用于2026丘成桐中学科学奖公示

To further validate the practical applicability of the sensing fabric, the sensing fibers and the fabric were separately used to monitor the bending of human fingers, elbows, and knees. As shown in **Figure 4c**, the sensors were attached to joints including the fingers, elbows, and knees, and changes in the electrical signals were recorded in real time during bending movements. The results showed that the sensing devices could detect different magnitudes of mechanical stress during different body movements, confirming the adaptability of these flexible devices to dynamic movements at multiple body sites and their capability for continuous monitoring.

Figure 4d illustrates the working principle of the sensing fabric. Analog signals from individual sensing nodes are acquired through point-to-point connections into register arrays, read out by progressive scanning as sequential signals, conditioned by analog circuitry, processed by a microcontroller, and transmitted via a Bluetooth transceiver to a computer or mobile device for decoding and reliable recognition.

On this basis, we applied the fabric sensor to human–robot motion mirroring (**Figure 4e, f**). Worn on joints such as the arm, it captured motion signals; integrated circuitry for acquisition, analog-to-digital conversion, and wireless transmission sent them to a miniature robot, which synchronously reproduced human joint movements. This demonstrates a complete chain from sensing and signal processing to motion recognition and remote actuation.

The future applications of motion mirroring lie in its ability to replicate human natural movements in real time onto robots, avatars, or remote devices, thereby serving areas such as remote operations in hazardous environments, telemedicine and surgery, rehabilitation training, industrial human–robot collaboration, intelligent prostheses and assistive control for people with disabilities, virtual reality/metaverse interaction, and

2026 S.-T. Yau High School Science Award
仅用于2026丘成桐中学科学奖论文公示

the digital transfer of motor skills. With advances in low-latency communication, flexible sensing, and AI recognition, motion mirroring is expected to become an important interface for human–machine integration, enabling humans to transcend distance, physical limitations, and constraints on manipulation precision, and to control external systems in a more natural and intuitive way.

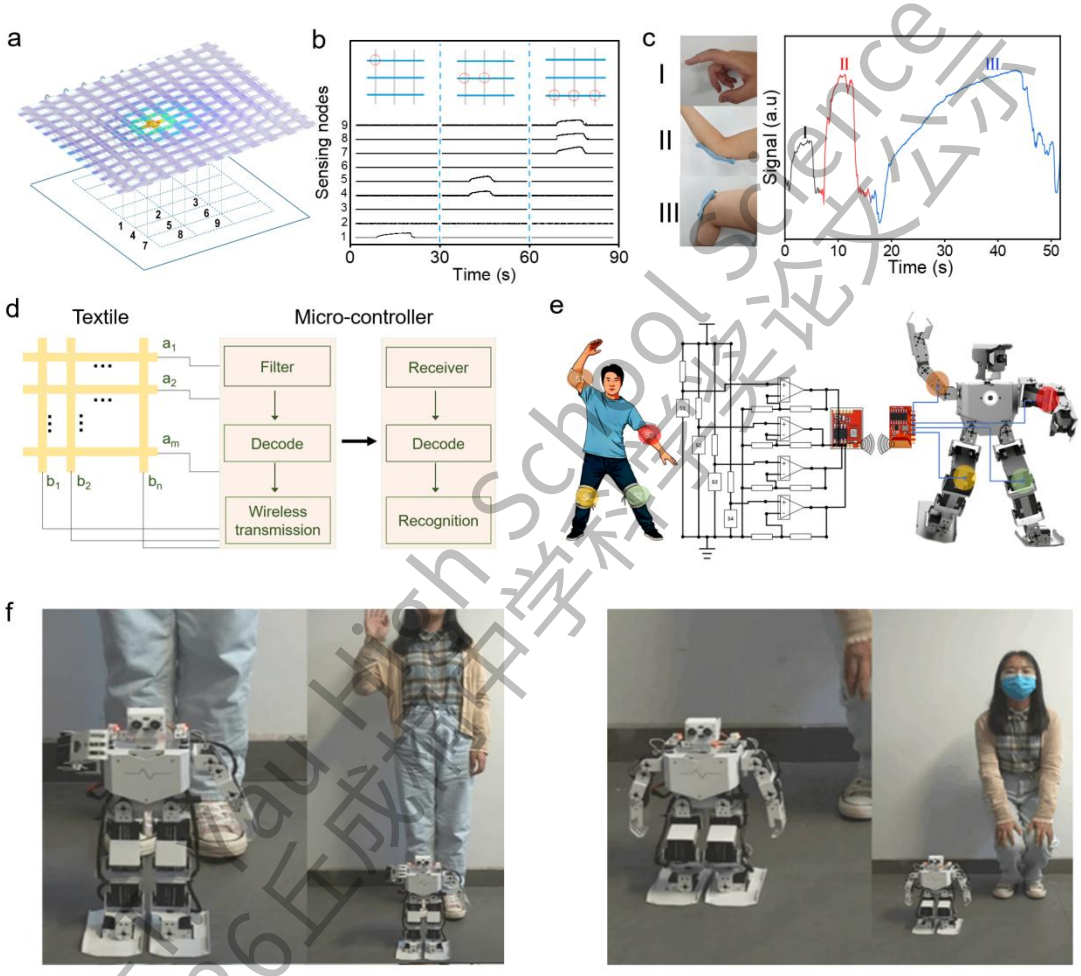


Figure 4. Demonstration of the sensing fabric. (a) Schematic illustration of the fabric-structured sensing array and the distribution of sensing nodes. (b) Real-time electrical signal responses of nine sensing nodes under continuous dynamic stimuli. (c) Signal characteristics of the sensor in response to different joint motions (finger, elbow, and knee). (d) Block diagram of the signal acquisition, wireless transmission, and motion recognition process of the wearable sensing system. (e) Schematic illustration of the real-time human–machine mirrored interaction system based on the fabric sensor

2026 S. Yau High School Science Award
仅用于2026丘成桐中学科学奖论文公示

and a miniature robot. (f) Photographs demonstrating the robot synchronously mimicking human motions (raising hand, and squatting).

3. Conclusions

In summary, we proposed an electric field-induced selective crystal facet growth strategy that enables the scalable fabrication of nano-arrayed oxide/polymer composite fibers at room temperature and atmospheric pressure. By simply introducing an auxiliary electrode into a continuous-flow fiber coating process, a meter-scale cotton thread coated with a ZnO nanoneedle array was fabricated and then woven into a fully addressable haptic fabric for wearable kinesthetic communication and human–metaverse interfaces. The nano-array structure increased sensitivity by 50%, and the performance remained almost unchanged over 2000 bending cycles. By wearing such a fabric, mirrored interaction between a small robot and human motion was demonstrated. Looking ahead, motion mirroring could replicate natural human movements in real time onto robots, avatars, or remote devices, enabling teleoperation in hazardous environments, telemedicine and surgery, rehabilitation training, industrial human–robot collaboration, intelligent prostheses and assistive control, VR/metaverse interaction, and digital transfer of motor skills. With advances in low-latency communication, flexible sensing, and AI recognition, such mirrored interfaces may become central to human–machine integration. This strategy is therefore expected to be extended to the scalable fabrication of other fiber materials, paving the way for commercial applications of electronic fabrics in embodied intelligence and related fields.

2026 S. T. Yau High School Science Award
仅用于2026丘成桐中学科学奖论文公示

4. Experimental section

4.1 Continuous fabrication of ZnO composite fibers

0.04 mol/L zinc acetate and hexamethylenetetramine (HMT) solutions were prepared and stored at a constant temperature of 10 °C after preparation. 60 mL of each of the zinc acetate and HMT solutions was measured into a beaker, and the beaker was placed in a thermostatic stirrer, where the mixture was mixed uniformly and maintained at 10 °C. The cleaned long-fiber substrate was passed through a mobile electrodeposition tank, its two ends were fixed on clamps, and the circuit was connected. Then, the mixed solution at 10 °C was poured into a mobile oxide electric-assisted deposition tank, and the moving speed of the electric-assisted deposition tank was adjusted for deposition. After deposition, the sample was rapidly blow-dried using a hair dryer to obtain a long-fiber ZnO composite electrode.

4.2 Fabrication of wire-type tensile stress sensors

The CNT slurry was made from a 3:1 weight ratio of CNT (Kuraray, YP-50f): PVDF mixture inside the 1-methyl-2-pyrrolidone solution. It was further deposited on an elastic wire, of which the two ends were respectively stuck to two cotton wires. Each end of the CNT-coated elastic wire was led out by coaxially coating a layer of MWCNTs, to form two conductive terminals on the cotton wire.

4.3 Weaving process for the sensing fabric

A sensing fabric was fabricated by a weaving process in which cotton yarns were used as the warp and composite fiber electrodes were used as the weft. First, the cotton warp yarns were arranged on a loom, threaded through the heddles and reed, and uniformly tensioned. The composite fiber electrodes were then mounted as weft yarns. During

2026 S. T. Yau High School Science Award
仅用于2026丘成桐中学科学奖论文公示

weaving, each composite fiber electrode was inserted across the cotton warp yarns and interlaced in a plain-weave pattern to form a woven fabric, in which the composite fiber electrodes served as the sensing units and the cotton yarns provided mechanical support and insulation. The weaving process was repeated to obtain a fabric with controlled electrode spacing and fabric density. After weaving, the fabric was removed from the loom, and the exposed ends of the composite fiber electrodes were connected to conductive wires for subsequent electrical measurements. The resulting woven sensing fabric was then cut and fixed for further characterization and sensing tests.

4.4 Characterizations and measurements

The morphology of the electrode was characterized using scanning electron microscopy (SEM) (S570, Hitachi). The photo-electrochemical tests were recorded in the electrochemical working station (CHI660D, Shanghai Chenhua). Simulation of the electric field distribution was done by COMSOL Multiphysics.

2026 S.-T. Yau High School Science Award
仅用于2026丘成桐中学科学奖公示

5. References

[1] Brasier, N. et al. Applied body-fluid analysis by wearable devices. Nature, 636, 57–68 (2024).

[2] Liu, J. et al. Bioresorbable, shape-adaptive structures for ultrasonic monitoring of deep-tissue homeostasis. Science, 383, 1096–1103 (2024).

[3] Hu, H. et al. A wearable cardiac ultrasound imager. Nature, 613, 667–675 (2023).

[4] Kadirvelu, B. et al. A wearable motion capture suit and machine learning predict disease progression in Friedreich's ataxia. Nat.Med., 29, 86–94 (2023).

[5] Narasimhan, M. et al. Self-care interventions for women's health and well-being. Nat. Med., 30, 660–669 (2024).

[6] Shao, B. et al. Large-area noise-resilient multiplexing triboelectric biomechanical sensing on clothing for high-precision full-body motion capture in wearables. Adv. Sci., 6, e77038 (2026).

[7] Yang, Y. et al. A non-printed integrated-circuit textile for wireless theranostics. Nat. Commun., 12, 4876 (2021).

[8] Zhu, H. et al. Tin perovskite transistors and complementary circuits based on A-site cation engineering. Nat. Electron., 6, 650–657(2023).

[9] Ding, S. et al. Afingertip-wearable microgrid system for autono-mous energy management and metabolic monitoring. Nat. Electron., 7, 1–12 (2024).

[10] Xu, S. et al. Skin sensors are the future of health care. Nature, 571, 319–321 (2019).

[11] Xu, C. et al. A physicochemical-sensing electronic skin for stress response

2026 S.-T. Yau High School Science Award
仅用于2026丘成桐中学科学奖论文公示

monitoring. Nat. Electron., 7, 168–179 (2024).

[12] Arwani, R. T. et al. Stretchable ionic-electronic bilayer hydrogel electronics enable in situ detection of solid-state epidermal bio-markers. Nat. Mater., 23, 1–8 (2024).

[13] Arab, K. et al. Advanced conductive fabrics: from nanomaterial integration to wearable applications. Adv. Compos. Hybrid Mater., 9, 213 (2026).

[14] Suryaprabha, T. et al. Hierarchical MXene/ZnO nanorods: WO3/CNT trilayer coatings on cotton for high-performance multifunctional wearable fabrics. Adv. Sci., 13, 25 (2026).

[15] Moradi, A. et al. Scalable and multifunctional PAN-MXene composite fibers for thermal management, photothermal conversion, energy harvesting, and sensing for wearable applications. Adv. Mater., 38, 26 (2026).

[16] Kim, J. et al. Hierarchically plied mechano-electrochemical energy harvesting using a scalable kinematic sensing fabric woven from a graphene-coated commercial cotton yarn. Nano Letters, 23, 7623-7632 (2023).

[17] Kim, J. et al. Ultrathin soft wearable sensor materials and structures: a review of current trends and prospectives. ACS Appl. Mater. Interfaces, 17, 59994-60027 (2025).

[18] Jia, Y. et al. High-energy-density aqueous magnesium metal battery fabrics enable ultrasensitive pressure sensing across 40° to 100°C. Sci. Adv., 12, 24 (2026).

[19] Gong, S. et al. Hierarchically resistive skins as specific and multi-metric on-throat wearable biosensors. Nat. Nanotech., 18,889–897 (2023).

2026 S.-T. Yau High School Science Award
仅用于2026丘成桐中学科学奖论文公示

[20] Hu, P. et al. Robust andflame-retardant zylon aerogelfibers for wearablethermalinsulationandsensingingarshenvironment. Adv.Mater., 36, 2310023 (2024).

[21] Seyedin, S. et al. Fibre electronics: towards scaled-up manufacturing of integrated E-fabric systems. Nanoscale, 13, 12818-12847 (2021).

[22] Yao, K. et al. Encoding of tactile information in hand via skin-integrated wireless haptic interface. Nat. Mach. Intell., 4, 893–903 (2022).

[23] Chen, G. et al. Electronic textiles for wearable point-of-care systems. Chem. Rev., 122, 3259–3291 (2022).

[24] Fang, Y. et al. Ambulatory cardiovascular monitoring via a machine-learning-assisted textile triboelectric sensor. Adv. Mater., 33, 2104178 (2021).

[25] Utsumi, S. et al. Giant nanomechanical energy storage capacity in twisted single-walled carbon nanotube ropes. Nat. Nanotech., 19,1–9 (2024).

2026 S.-T. Yau High School Science Award
仅用于2026丘成桐中学科学奖论文公示

6. Acknowledgements

The authors acknowledge the Chongqing Young Eagle Program Student Special Research Candidate Project, and thank Juan Pei, Yao Li, and others from Chongqing University, as well as Siwei Xiang from the Chongqing Institute of Green and Intelligent Technology, Chinese Academy of Sciences, for their assistance and valuable suggestions regarding the human–machine mirror interaction experiments.

（1）背景与指导关系说明

本项目依托重庆市雏鹰计划学员专题研究备选课题。“雏鹰计划”是重庆市教委面向普通高中学生实施的创新人才培养计划，通过选拔学有余力的学生进入高校、科研院所实验室，在高校导师与中学教师双师指导下开展为期两年的专题课题研究，以培养拔尖创新后备人才。在本项目中，重庆大学范兴教授担任高校指导老师，重庆市巴蜀中学校王旭老师担任中学指导教师，全程参与项目研究指导工作。重庆市巴蜀中学校周子涵、许知微、颜子皓为项目组成员。其中，范兴老师在选题方向、实验设计、材料合成、数据分析和论文写作中提供系统指导，属于无偿指导，不领取额外报酬。王旭老师作为校内指导老师，立足中学生科研特点，全程参与课题选题打磨、实验数据校核、内容优化等关键工作，协助团队梳理研究逻辑、规范科研流程，同时负责统筹完善论文修改等文本工作，保障项目研究有序推进、成果规范落地。参赛学生周子涵、许知微、颜子皓为论文共同作者，承担核心实验、数据分析与论文撰写。重庆大学裴娟、李钥等人，以及中国科学院重庆绿色智能技术研究院项思维等人，在人机镜像交互实验中提供帮助和建议，属于他人协助，已在致谢中说明；他们未参与核心材料合成、表征和论文主要撰写。

2026 T-Yau High School Science Award
仅用于2026丘成桐中学科学奖论文公示

（2）整体研究过程与分工说明

选题来源：项目源于重庆市雏鹰计划学员专题研究备选课题，针对可穿戴电子的实际应用需求，确定化学领域的“纳米复合纤维材料批量化制备”研究方向。选题确立过程中，王旭老师结合中学生科研创新赛事要求与研究可行性，协助团队优化选题切入点，规避研究难点、明晰研究核心与创新点，保障选题兼具学术价值与实践落地性。

实验设计及实施：在整个实验过程中，范兴老师统筹指导总体方案，包括指导材料合成、数据分析和论文修改；王旭老师重点负责选题落地指导、实验数据整理与分析方法指导，协助学生规范数据处理流程、校核实验结论，同时针对性指导论文选题优化、框架调整，完善论文致谢等附属内容，规范科研成果呈现形式；周子涵负责材料合成、数据处理、论文写作；许知微负责材料表征、性能测试、论文写作；颜子皓负责数据处理、论文写作和文献整理。人机镜像交互实验中，团队设计信号采集、模数转换和无线传输电路，并在裴娟、李钥、项思维等人的协助下，完成小型机器人与人体动作的同步镜像演示。

（3）关于使用 AI 情况的说明

在开展本研究项目的过程中，团队成员在指导教师的允许下，仅使用 AI（DeepSeek）作为辅助工具，用于研究报告写作（2026 年 7 月 21 日-2026 年 9 月 13 日，使用频率：10h/周）的文献资料查找、写作思路优化、语言翻译及润色等辅助性工作，所有 AI 生成或建议内容均经团队成员人工审核、修改、验证。研究报告的选题构思、研究设计、核心论证、实验数据及学术表达等主体部分，全部由团队成员完成。除本说明列明的情况外，未在该成果中使用其他 AI 工具

2026 S.T. Yau High School Science Award
仅用于2026丘成桐中学科学奖公示

或服务。

所有使用 AI 的相关聊天记录详见附件“其他材料”。

2026 S.-T. Yau High School Science Award
仅用于2026丘成桐中学科学奖论文公示